

EMAT-Based Inspection of Natural Gas Pipelines for Stress Corrosion Cracks

Venugopal K. Varma¹, Raymond W. Tucker, Jr., and Austin P. Albright
Oak Ridge National Laboratory
Oak Ridge, Tennessee 37831
USA

Abstract

This paper describes the wavelet-based analysis of electromagnetic acoustic transducer (EMAT) signals for in-line inspection of flaws in a 30-inch-diameter natural gas pipeline. The sensor is capable of detecting physical flaws (e.g., stress corrosion cracks, circumferential and axial flaws, and corrosion) in the walls of gas pipelines. Using an in-line non-contact EMAT transmitter–receiver pair, flaws can be detected in the walls of a pipe that the more commonly used magnetic flux leakage technology has problems detecting. One EMAT is used as a transmitter, exciting an ultrasonic impulse into the pipe wall, while the second EMAT, located a few inches away from the first, is used as a receiving transducer.

Using the 58-coefficient Symlet wavelet with 4-level (scale) wavelet decomposition, the EMAT data were analyzed. The first-level detail was not used in any of the algorithms, but the other resulting wavelet levels were used in different combinations to calculate a vectorized feature set for comparing “flaw” and “no-flaw” signals. “Entropy,” “energy,” and a “difference measure” were the various attributes evaluated to differentiate the “flaw” and “no-flaw” signals. The results using this approach have shown promise for EMAT measurements obtained from a translating pipe inspection gauge. There are still issues that need further research: establishing the ability to differentiate flaw types and quantifying the sensitivity of the EMAT measurements.

¹ Corresponding author (varmavk@ornl.gov)

1. BACKGROUND

The integrity of the gas pipelines needs to be monitored frequently by pipeline operators to mitigate potential hazardous conditions. With more than 90% of the pipelines buried underground, locating potential flaws is a major challenge. In-line inspection technologies are necessary to locate the flaws without having to resort to excavation. Once the operator knows of suspected areas where flaws might exist, hydrostatic testing can be performed.

Stress corrosion cracks (SCCs) in pipes are influenced by both environment and stress [1, 2]. Initially, corrosion begins when water comes into contact with steel where disbondment of the protective coating has taken place. Once cyclical loading, temperature, residual stress, and bending load act on the initial corrosion site, a crack or a colony of cracks can develop. Without stress, the corrosion area will not transform into a crack. Cracks in the pipelines can reduce the integrity of the pipe and hence reduce its potential service life.

In a laboratory environment, SCCs can be easily detected using liquid fluorescent magnetic particle inspection. However, this technique is not practical for in-line inspection of pipes. ORNL has developed a shear horizontal (SH) wave electromagnetic acoustic transducer (EMAT) system for the inspection of pipelines. The SH-mode EMAT is used in a circumferentially oriented configuration since the main objective of this system is to detect SCCs that are axially oriented along the length of the pipes. Magnetic flux leakage (MFL), which is a mainstay of the in-line pipe inspection industry, has difficulty detecting axially oriented cracks. Although there have been some developments in the area of liquid-filled wheel probes using ultrasonic shear waves, they do not offer reliable detection of cracks. Hence, the EMAT technique is being pursued as an alternative tool to detect SCCs.

2. ORNL EMAT SENSOR DEVELOPMENT

Effective in-line inspection techniques exist to detect corrosion, mechanical damage, and wall thinning, detecting SCCs still poses a problem. Oak Ridge National Laboratory (ORNL) has developed an EMAT system that uses SH-guided wave to detect SCC.

ORNL uses EMATs configured in “through-transmission mode” for SCC detection. In through-transmission mode, the transmitted wave is generated by one EMAT and received by another. Hence, independent of the location of the flaws, the ultrasonic waveform arrives at the receiver within a fixed time window since the distance between the receiver and the transmitter does not change. In “pulse-echo” mode, a single EMAT acts as both the transmitter and the receiver. The reflected signal is what is collected and analyzed. The characteristics of the signal received will be dependent on the location of the flaw from the transmitter. This dependency will cause a phase shift and attenuation of the signal. Hence, the pulse-echo mode is more difficult to implement for a pipe inspection gauge (PIG) that is translating through a pipe. To simplify the flaw analysis, only “through-transmission” mode was used in this project. Later on, to clearly identify

the location of the flaws on the circumference of a pipe and obtain another signal from the same flaw location, “pulse-echo” mode might be incorporated into the design along with “through-transmission.”

The pipeline industry is interested in detecting SCCs in transmission pipelines because the larger-diameter pipes carry large fuel volumes and the potential for greater damage exists when a pipe failure occurs. The ORNL EMATs are configured to detect flaws in 30-inch pipes. Figure 1 is a photo of the EMAT-based pipe test equipment. The main body of the test fixture is made of 80/20® aluminum and travels within the pipe on roller-blade wheels. The pair of EMATs that act as the sensing unit are attached to the frame. The EMATs have a pre-adjusted standoff distance from the pipe inside diameter of about 0.010–inch that is maintained by using a set of small roller wheels located on the sensor head mount. Independently mounted springs also allow the sensors to negotiate uneven surfaces of the pipe without damaging the EMAT head while maintaining distance to the inside wall surface. A resolver is used to measure the distance traveled by the inspection system while traveling inside the pipe. The circumferential separation between the transmitter and the receiver EMAT can be adjusted, and the current setting of 8 inches ensures that the excitation signal does not overlap with the transmitted chirp signal. To ensure that the PIG does not rotate circumferentially while traveling inside the pipe, a counterbalance weight is used that can be adjusted to make the PIG travel in a straight line.

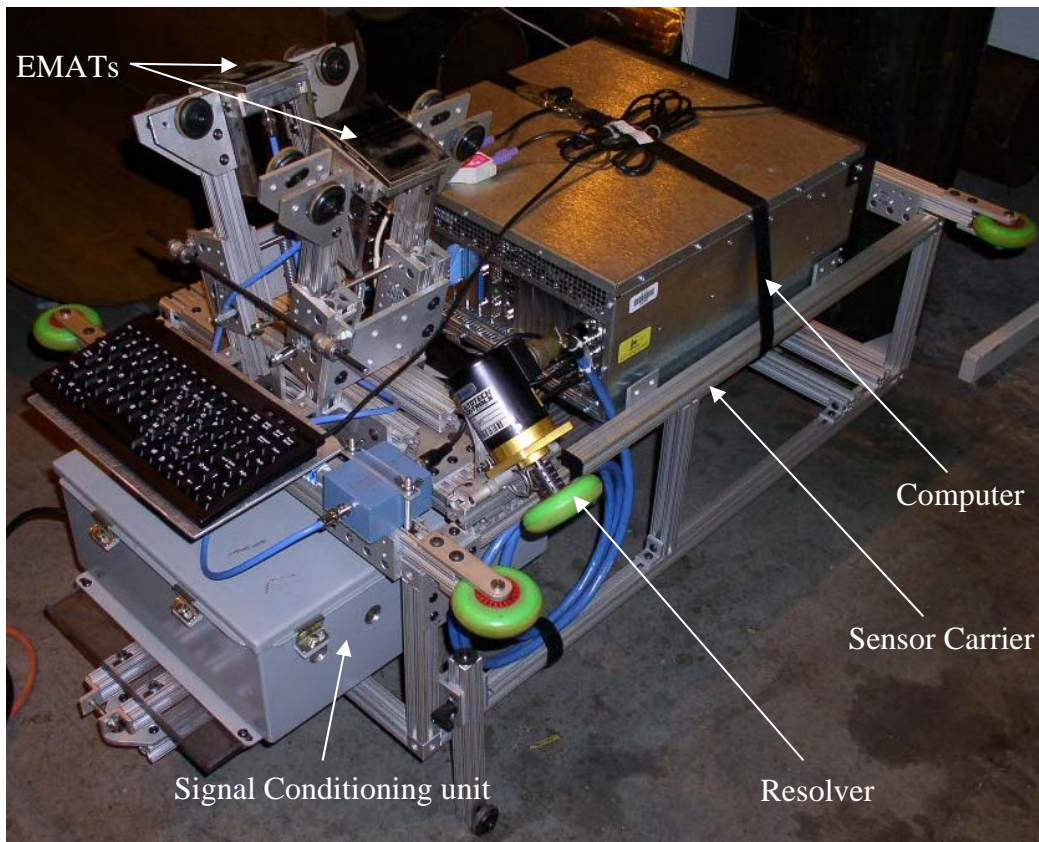


Figure 1. ORNL PIG with EMAT sensors for inspecting a 30-inch diameter pipe.

A windowed SH ultrasonic wave (22 microsecond in duration) is generated every 12 milliseconds and is sampled at a 5-MHz sample frequency by the data acquisition system. The data acquisition system collects both resolve position and the EMAT waveform signal at the rising edge of every trigger signal from the tone-burst card. A LabView® program is used to gather the data from the data acquisition board and write them to a file on the hard disk.

The current set up is used to evaluate the defects that exist in an 8-inch circumferential distance between the transmitter and the receiver EMATs. The receiver EMAT on the 30-inch pipe wall will also obtain the signal that is traveling the 85.25-inch circumferential path, but this signal is too weak to be used for flaw classification. Hence, for a field-deployable flaw classification and characterization PIG, multiple pairs of EMATs will have to be deployed.

3. WAVELET ANALYSIS

3.1. Introduction

The wavelet function $\psi(t)$ is any complex-valued function ψ of a complex variable that meets two conditions. First, the function has a zero average value; hence, it must oscillate. Second, it must have finite energy; hence, it must be a windowed burst. Infinitely many functions meet these conditions, but only a fraction of that infinitude is useful for engineering applications.

Unlike the Fourier transform, which represents signals as an infinite series of sinusoidal waveforms, the wavelet transform represents a signal with a finite series of wavelets. Since the signal of interest is a finite-energy tone burst, it is more logical to use a wavelet instead of a Fourier series to analyze the problem.

3.2. Preprocessing of Data

The signature obtained from the data acquisition board is stored in a binary file to reduce the disk space utilized. Data are collected for every rising trigger signal from the tone-burst card, which coincides with the excitation signal sent to the transmitter. Although under ideal conditions, all signatures collected should be acceptable, there are cases where the data becomes corrupted in field deployment. The corruption of data could be from amplitude or phase errors or a synchronization problem between the trigger and tone burst (see Figure 2).

To remedy this problem, a pre-cleaning routine was developed. In Figure 2, a “no-flaw” signal is subdivided into excitation, head, signal, and tail sections. The energy content in each of the four areas is used to determine if corruption has occurred. The essential part of the pre-cleaning was to look at the ratio of the energies in the head and tail sections of the signal to the excitation energy in the received signal. The “head/excitation” and “tail/excitation” fractions become pronounced when there is a

synchronization problem or an amplitude error. To eliminate phase errors, an uncorrupted signal is correlated with all other signals collected. When the correlation is bad, the data set has phase errors. After the initial cleaning of the data set, wavelet analysis is performed. When the EMATs traverse a flaw region, the ultrasonic wave is reflected and dispersed. Figure 3 depicts a typical EMAT signature over a flaw region. Looking at Figure 3, one sees some amplitude reduction and shape change. These

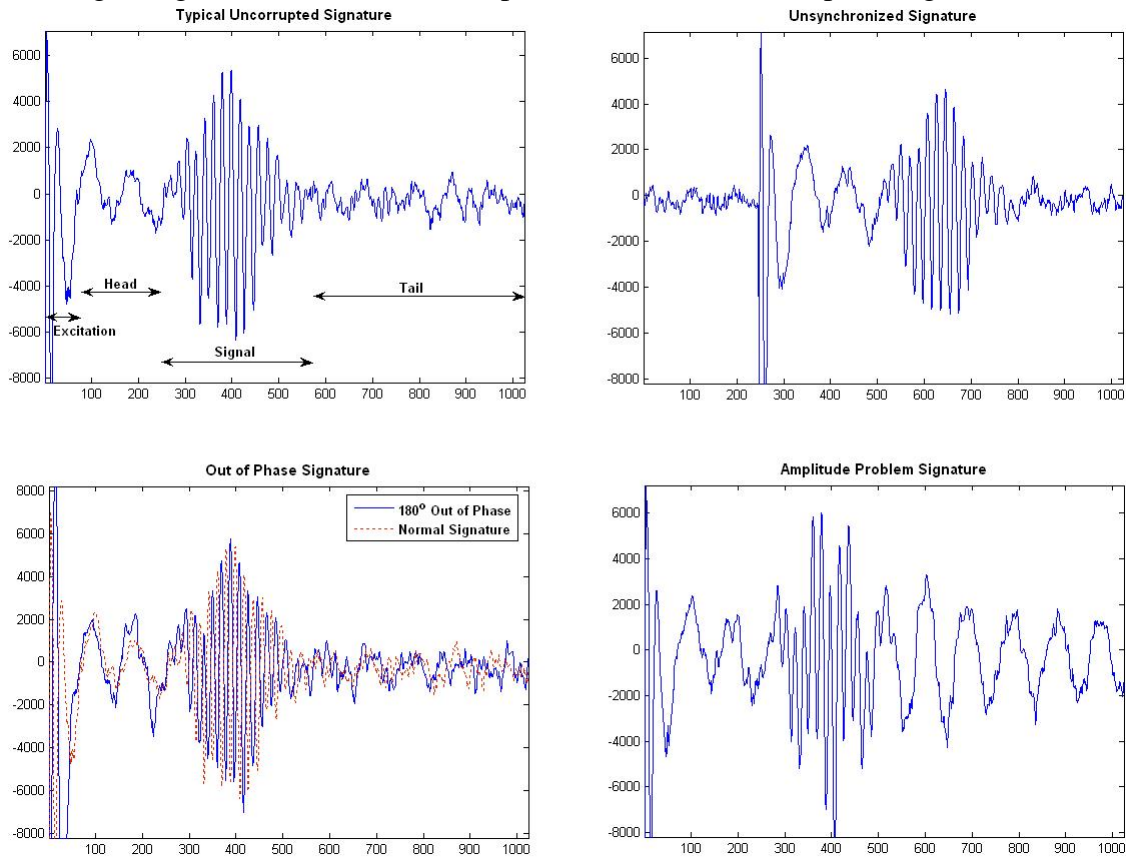


Figure 2. Signals from EMAT (uncorrupted and corrupted).

changes are discussed in the development of the signal analysis explained in the next section.

3.3. Development of Feature Set

A 58-coefficient Symlet wavelet was used for the signature analysis [3, 4, 5]. The signal was decomposed into four wavelet scales. Each sampled waveform consists of 1024 samples. Only a portion of the signal samples from 270 to 781 (512 data points) were used for the wavelet analyses. After the approximations and details are generated, features are defined to extract information that enables a “flaw” to be differentiated from a “no-flaw” signal.

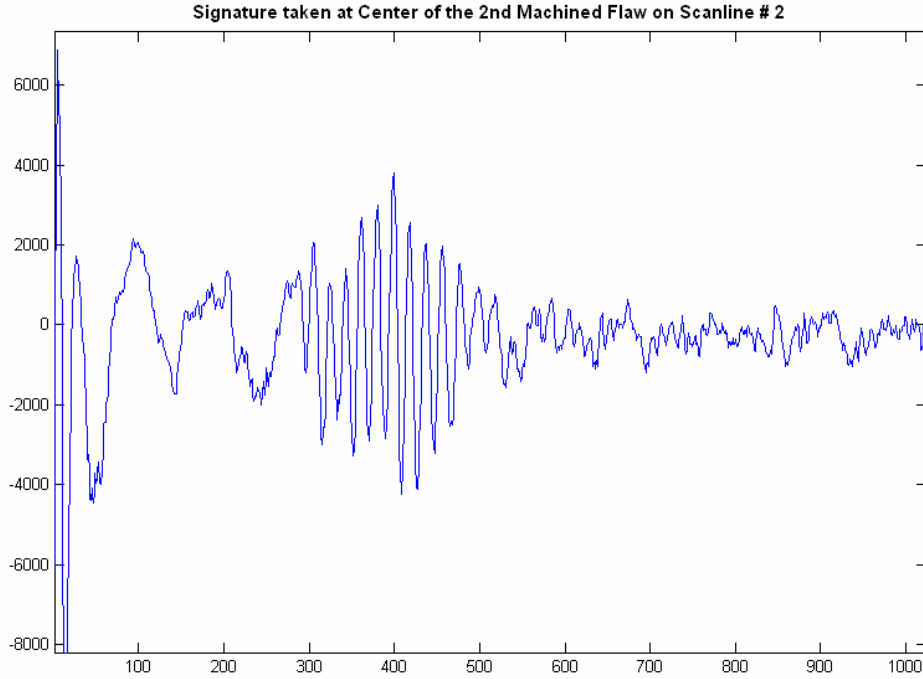


Figure 3. Raw signature over a machined flaw.

In this analysis “energy,” “entropy,” and “difference measure” were used as features. The analysis uses the deviation from a “no-flaw” signal to determine whether the signal being analyzed is from a flaw region. In order to perform the analysis, a good set of “no-flaw” signatures is needed. In the following description “SM” refers to the mean signal from the “no-flaw” data set that will be used in the following analysis. S_1 , S_2 , S_3 , and S_4 correspond to “detail2,” “detail3,” “detail4,” and “approximation4” wavelet scales, respectively, with “detail1” not being used in this analysis.

The feature sets that pertain to “energy” are given by

$$F_{ij} = \frac{\sum_{k=1}^n S_{ijk}^2}{\sum_{p=1}^j \sum_{k=1}^n S_{ijkp}^2}, \text{ for } j = 1, 2, 3, \text{ and } 4,$$

where S is the wavelet detail/approximation corresponding to signature i , i is the sample number, j corresponds to the detail/approximation scale, k corresponds to the data point at a particular scale, and n is the total number of data points at a particular scale.

The feature sets that pertain to “entropy” are given by

$$F_{ij} = \sum_{k=1}^n -S_{i(j-4)k} \ln(S_{i(j-4)k}), \text{ for } j = 5, 6, 7, \text{ and } 8.$$

Finally, the difference feature is defined as

$$F_{ij} = \sum_{k=1}^n (S_{i(j-5)k} - SM_{(j-5)k})^2, \text{ where } j = 9.$$

The feature matrix F is of dimension $(9 \times m)$, where m is the total number of signatures being analyzed. The relative magnitude of the values of each feature is different. In order to give each feature equal weighing when combined, it is necessary to normalize the values for each feature. The normalized vectors are given by

$$\bar{F}_{ij} = \frac{F_{ij}}{\text{Max}(F_i)}, \text{ where } i = 1, 2, 3, 4, \text{ or } 9$$

and

$$\bar{F}_{ij} = \frac{F_{ij}}{\text{Min}(F_i)}, \text{ where } i = 5, 6, 7 \text{ and } 8.$$

Here $\text{Max}(F_i)$ refers to the maximum value in the i^{th} row, and $\text{Min}(F_i)$ refers to the minimum value. Let the covariance of the matrix \bar{F} be defined as Γ . The covariance matrix quantifies the interdependences of the feature sets used. The Mahalanobis distance measure that combines all feature vectors into a single metric is then given by

$$M_i = [(F_{i1} - FM_1) \dots (F_{i9} - FM_9)] \Gamma^{-1} \begin{bmatrix} (F_{i1} - FM_1) \\ \cdot \\ \cdot \\ \cdot \\ (F_{i9} - FM_9) \end{bmatrix},$$

where FM corresponds to the mean feature vector derived from the reference “no-flaw” signature set and M_i corresponds to the Mahalanobis distance for the particular signature i . In calculating the Mahalanobis distance, the value of the mean ‘no-flaw’ feature is subtracted from the feature value being evaluated to obtain a deviation from the mean rather than the absolute value. Thus, deviation, and not the absolute value of the features, is used throughout the analysis.

3.4. SCC Determination on 30-inch-Diameter Pipe

To test the effectiveness of detecting SCCs on pipes, the EMAT test PIG was deployed in a 30-inch pipe that was 20.41 feet long at the Battelle pipeline simulation facility in Columbus, Ohio. Figure 4 shows the pipe that was used for this test. The pipe

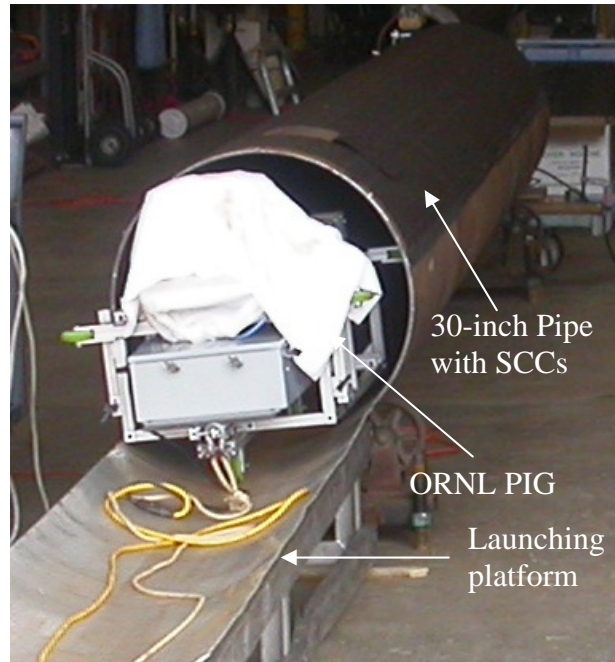


Figure 4. Sample pipe tested at Battelle.

contained many natural SCCs. The ORNL PIG was deployed at one end of the pipe and pulled through at constant velocity using a winch at the other end. The EMAT orientation was maintained correctly (axially) during the pull using a counterweight mechanism on the PIG. The counterweight prevented the PIG from rotating circumferentially as it moved through the pipe. The EMATs scanned axial lines along the length of the pipe during this testing. The EMAT sensors had the ability to detect SCCs on an 8-inch span on any particular scan line.

Figure 5 shows the Mahalanobis distance measurement for the EMAT signal obtained during testing. The pipe was made up of two sections of pipe welded together. There was a circumferential weld at 60 inches from the deployment end of the pipe. Figure 5.

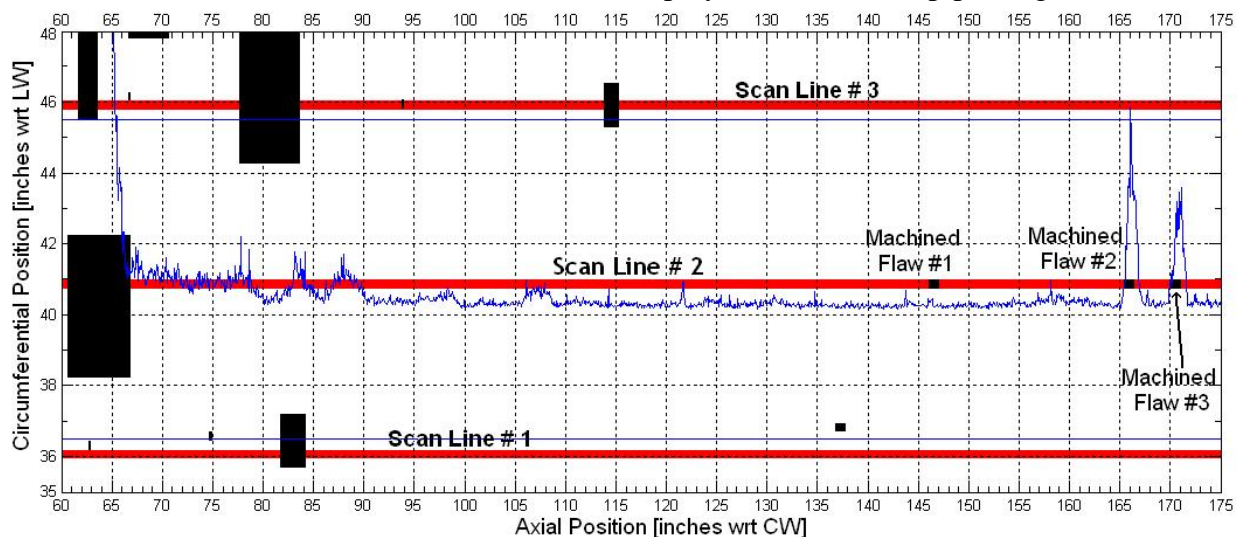


Figure 5. Mahalanobis distance measure for line #2 overlaid on pipe crack locations.

shows the results of the wavelet analysis on the pipe from 60 to 175 inches after the circumferential weld. The red lines are the scan lines used by the ORNL PIG to detect the SCCs.

The black boxes and marks indicate the location of colony of cracks or individual cracks along the pipe. Three machined flaws were used as reference flaws for the EMATs before testing. The machined flaw location and the EMAT prediction are shown in Table 1 and Figure 5.

As seen in Figure 5, the Mahalanobis distance measure for scan line #2 (blue line) is able to predict well (rise in value from the floor) the presence of flaws (black boxes and marks). There are some areas, however, where the blue line rises significantly above the floor level even though no flaws are present. Some of the spikes are the result of tar coating present on the pipe. This issue is discussed in detail in section 3.5.1.

The machined flaws were generated using a grinding wheel. As a result, the hole cross section is not rectangular but has the shape of a parabola. The peak of the Mahalanobis distance measure corresponds to the peak of the parabola. The depth of the flaw

Table 1. Calibrated machined flaw location and EMAT prediction

Machined flaw number	Calibrated flaw location (inches)	Length (inches)	Depth (% of wall thickness)	EMAT calculated location (inches)
#1	146.75	0.88	25	146.36
#2	166.06	1.212	48	166.06
#3	170.625	1.204	63	170.69

denoted in Table 1 refers to the depth of the deepest point. The predicted and the actual locations match well when comparing the location of the peaks, while the predicted length of the flaw tends to be greater than the actual flaw. The Mahalanobis distance plotted (blue line) in Figure 5 is the average of five sample runs. Therefore, although it is not easy to detect the position of Flaw #1 from Figure 5, it could be deciphered from individual Mahalanobis distance measures. The larger estimation of the flaw length results from the fact that the EMAT has an active region of 1.5×1.5 inches. Thus, when it traverses a flaw, the signal continues to be disrupted as long as the flaw is located between any portions of the active EMAT sensing region. This issue will be addressed in the next section with measurements taken on a 0.5-inch through-hole.

3.5. Measurements on a 0.5-inch Hole

For the data collected thus far, the ability to identify flaws was based on best-engineering practices and hypotheses derived from experimental data collected on assayed pipe sections removed from service. However, the false detection of cracks is unacceptable. In order to form a stringent set of criteria for flaw determination, a series of parametric tests were performed.

The objectives of these baseline parametric tests were as follows: determine (1) how a flaw of exactly controlled size is represented in the Mahalanobis distance; (2) how the size of the flaw correlates to its representation in the Mahalanobis distance measure; and (3) the active region between the transmitter and receiver EMATs where the flaw is detectable. The tests were performed on a 78.75-inch long, 30-inch-diameter pipe section that has never been in-service or exposed to any other adverse conditions. A 0.5-inch-diameter through-hole was drilled with the center of hole located at 38.625 inches from the end of the pipe from which the scans were commenced.

3.5.1. Flaw Location and Sizing

The new pipe had no natural defects present, and only a simulated flaw was machined. From the test, it was found that the Mahalanobis distance spiked to a value of over 1200 in response to the 0.5-inch-diameter hole, while the expected value of the distance stayed in the range of 20 to 40 for the entire pipe length. A flaw indication is defined as a significant deviation of the Mahalanobis distance from the baseline neighboring sections. The shape of the deviation for the 0.5-inch flaw is distinct, consisting of an abrupt rise in the error distance with a steep slope compared with the other three deviations (spikes #1, #2, and #3 spikes) present in the plot. The magnitudes of the three deviations, taken at the tip of the “triangles” where the majority of samples converge, are 150, 178, and 154 and are identified accordingly in Figure 6. The slopes of the spikes in Figure 5 that do not correspond to an identified flaw location are similarly less steep compared with the ones at the flaw locations.

The Mahalanobis distance response to the 0.5-inch-diameter hole occurred over a length of 3 inches as the EMATs traversed the pipe. This length of a flaw is measured from the point at which the error distance first starts to rise out of the expected range to the point that the error distance returns back to the expected range. The length is 2.5 inches longer than the actual diameter of the hole (see Figure 7). Figure 7 shows the deviation from the baseline for the 0.5-inch hole with the largest spike (#2) overlaid for perspective.

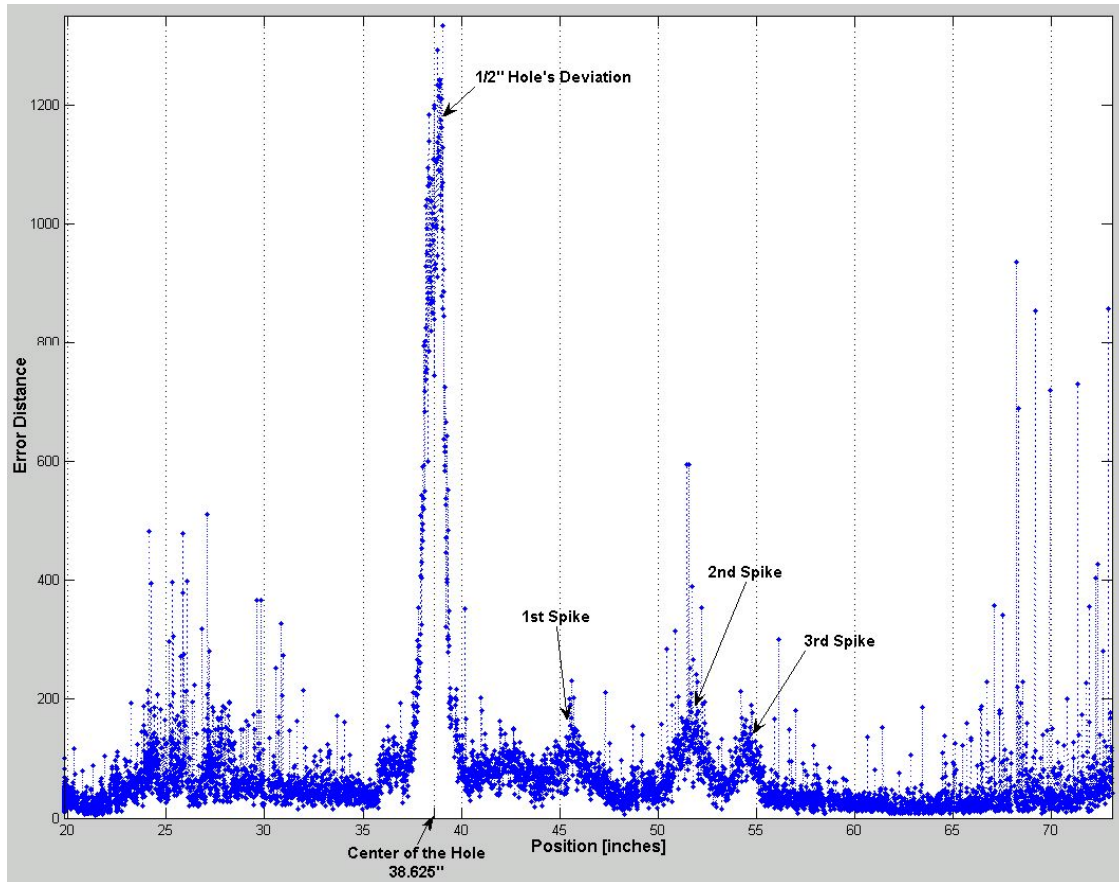


Figure 6. Mahalanobis distance measure for 0.5-inch-diameter hole at the center of transmitter and receiver EMATs.

3.5.2. Sensitivity to the Position of Flaw

Scans were taken to improve the knowledge of how the proximity of an EMAT to a flaw affects the resulting signature. This was achieved by reorienting the pipe so that the transmitter EMAT would have the 0.5-inch-diameter hole pass over it at three distinct locations. In Figure 8, these locations are referred to as the inner edge (Position 2), the middle section (Position 3), and the outer edge (Position 4).

To interpret the responsiveness of the EMAT in detecting the flaw, the resulting Mahalanobis distance for each orientation was compared with the one where the 0.5-inch hole passed through the center of the receiver and transmitter EMATs (Position 1 in Figure 8).

The detectability of the flaw with respect to a direct overpass of the EMAT is dependent upon the portion of the EMAT that passes directly over the flaw. As seen in the top right plot in Figure 9, the flaw is easily detectable when the inner portion of the EMAT passes over the defect. The slopes of the sides remain steep and defined with the peak of the response almost two orders of magnitude greater than the expected range. On the other hand, the middle section of the EMAT passes over the hole, the response is one-third of the magnitude compared with the inner-edge response (see Figure 9). The flaw is still detectable, and the response to the 0.5-inch

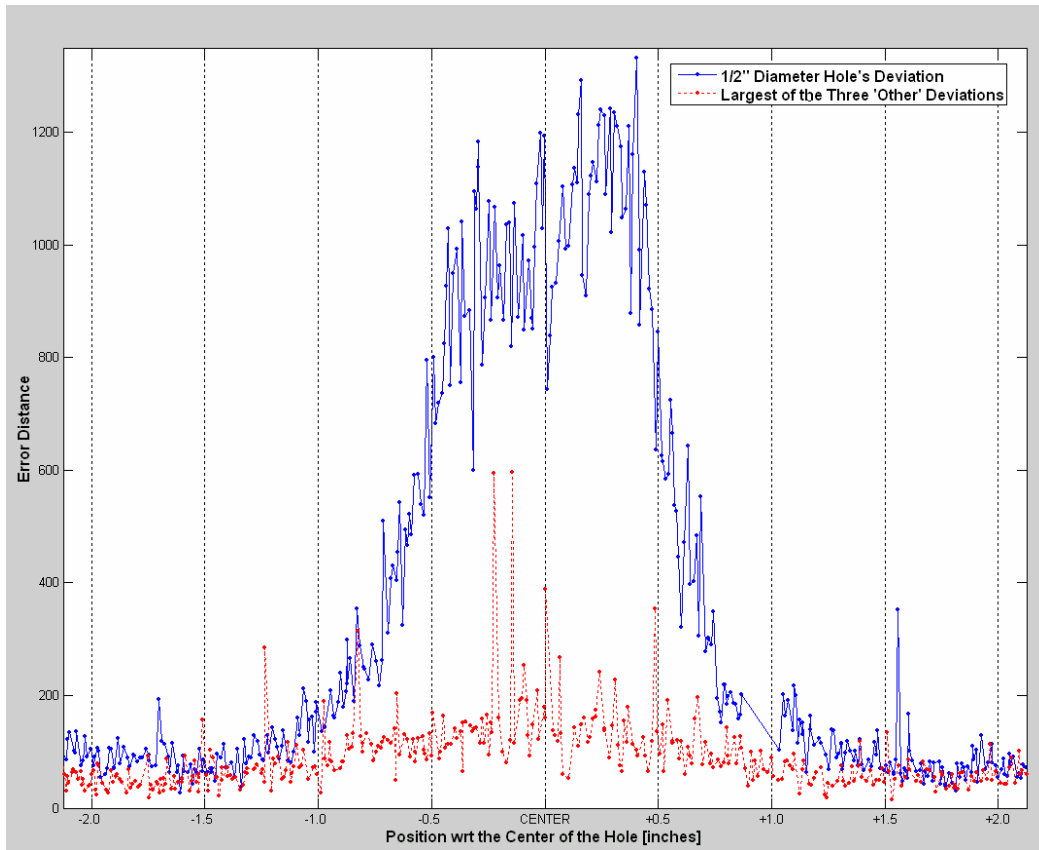


Figure 7. Mahalanobis distance for 0.5-inch-diameter hole overlaid with spike #3 response.

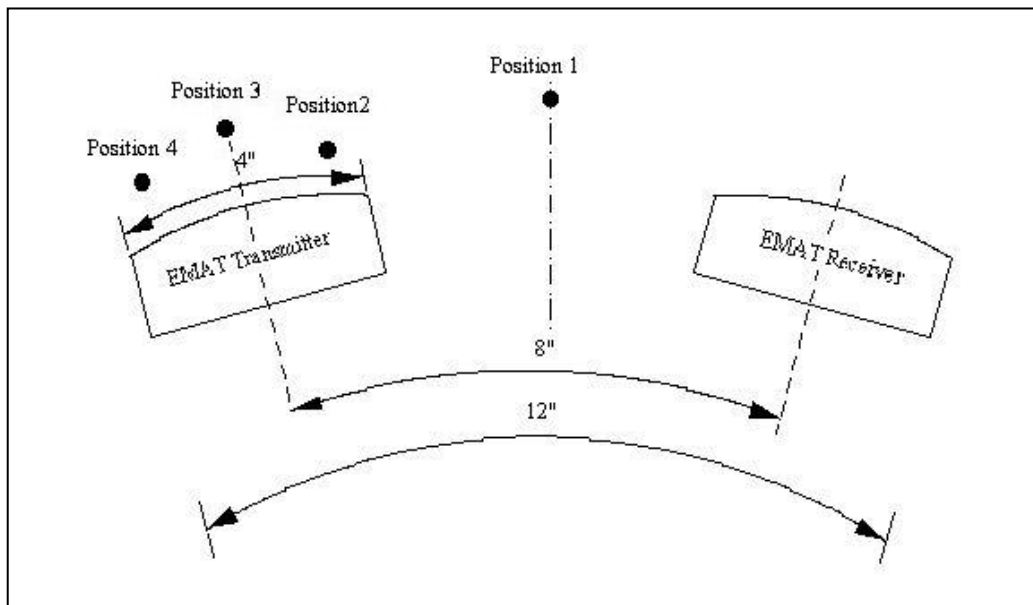


Figure 8. The four different orientations of the EMATs with respect to the 0.5-inch hole.

hole is well above the baseline. Although the slope of the Mahalanobis distance measure is less compared with the Position 1 and Position 2 responses, it is still greater than other spurious deviations observed (spike #1, #2, and #3).

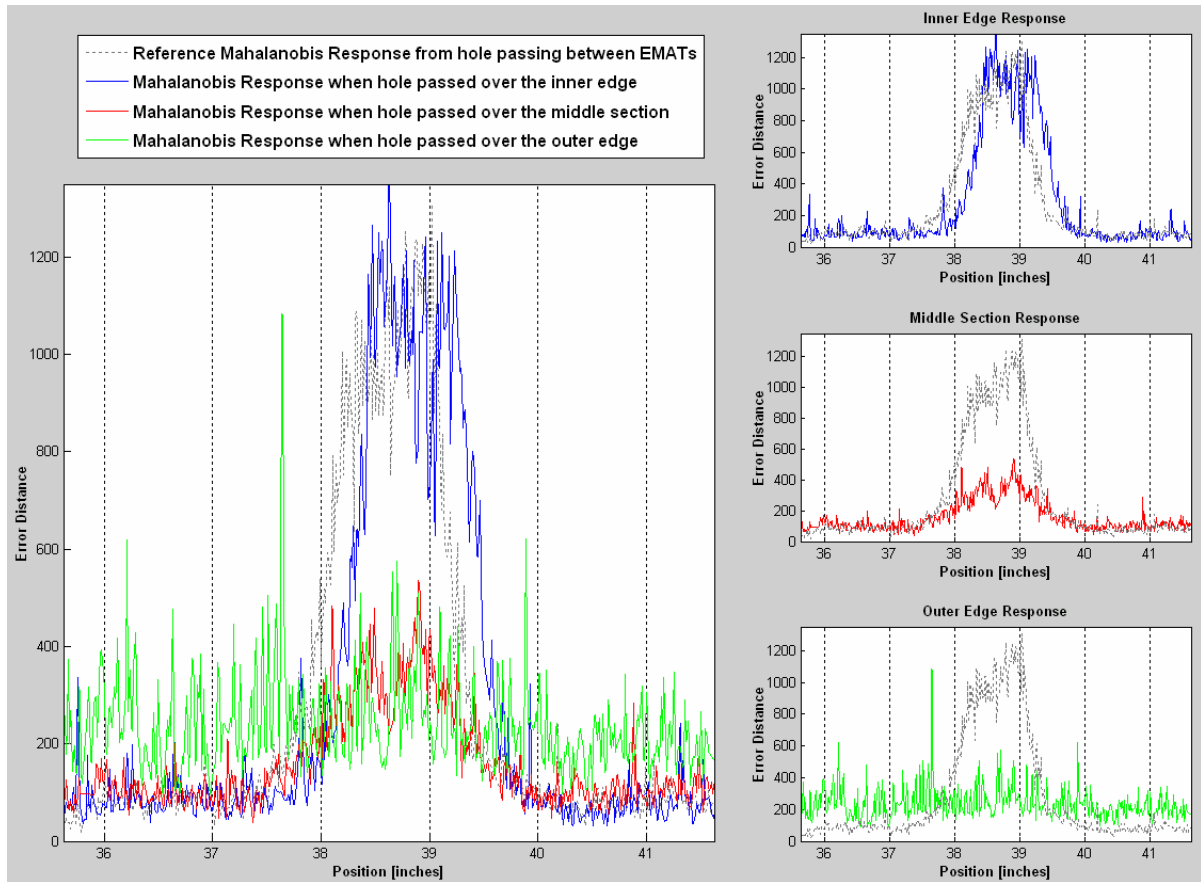


Figure 9. Plots of the Mahalanobis distance for 0.5-inch-diameter hole for different EMAT scan orientations.

The final pass over the outer section of the transmitter EMAT could not detect the machined flaw. As seen in the bottom right plot in Figure 9, there is no change in the baseline that corresponds to the location of the 0.5-inch hole.

The tests conducted have demonstrated that a flaw indication in the Mahalanobis distance generally exhibits two distinct characteristics: (1) it should be a minimum of several hundred points higher than the overall baseline range of values, and (2) the slopes of the sides of true flaw response should be dramatically steeper than any low-level deviation seen elsewhere in the same Mahalanobis distance measure. Also for a reliable detection, the flaw has to lie between the two inner sides of the EMATs (transmitter and receiver).

4. FUTURE RESEARCH AND DISCUSSIONS

Although the EMATs were able to detect SCC flaws and approximate their size, the depth of the cracks was not considered in our analysis. The EMAT's effectiveness in

detecting a crack is directly proportional to the depth of the crack. The width of a crack has effect on the signal, but the system will not be able to detect the difference between two cracks and a single wide crack if all other parameters are held the same. If the depth of a crack changes in a particular flaw location, the EMAT's greatest response will be centered on the deepest crack location and not the center of the gross size of the crack. The current method of detecting SCCs in pipelines using liquid fluorescent magnetic particle inspection cannot determine the severity (depth) of the crack. In the tests conducted so far, we could not correlate the results with the severity (i.e., depth) of the flaw since these data were missing from our sample. A liquid dye penetrant X-Ray is needed to correlate the results obtained. The current ORNL-configured EMATs are unable to detect flaw depth smaller than 15% of the pipe wall thickness. Increasing the power of the tone-burst card could improve this sensitivity.

The EMAT signal becomes greatly attenuated in the presence of tar coating. Methods need to be developed to overcome this problem to make EMAT detections a more desirable approach. Weld effects were another problem faced in these early experiments. However, refinement of the algorithm should be sufficient to overcome this problem since all relevant information is present in the received signal. A better way to extract this information is all that needs to be developed.

5. CONCLUSIONS

The EMAT-based inspection system was designed and tested on a 30-inch-diameter pipe with natural SCCs. The wavelet algorithms developed to predict the location of the defects have successfully been able to identify the cracks. Using the discrete wavelet transform and decomposing the signal into four wavelet scales, feature vectors were developed that could distinguish between "flaw" and "no-flaw" regions. Further refinements are needed on the wavelet algorithms to differentiate between different types of flaws and correlate the results to depth of SCC flaws. These refinements are currently being pursued at ORNL to improve the EMAT flaw detection capability.

6. ACKNOWLEDGEMENT

This work was supported by the DOE National Energy Technology Laboratory (NETL), Strategic Center for Natural Gas. The work was performed at Oak Ridge National Laboratory, which is managed and operated by UT-Battelle, LLC., for the U.S. Department of Energy under Contract No. DE-AC05-00OR22725.

References

1. Leis, B.N., and Eiber, R.J., "Stress-Corrosion Cracking on Gas-Transmission Pipelines: History, Causes, and Mitigation," Proceedings of First International Business Conference on Onshore Pipelines, Berlin, December 1997.
2. Ginzler, R.K., and Kanters, W.A., "Pipeline Corrosion and Cracking and the Associated Calibration Consideration for Same Side Sizing Applications," *NDT.net* Vol.7, No.07 (July 2002).
3. Kercel, S.W., Tucker, R.W., and Varma, V.K., "Pipeline Flaw Detection with Wavelet Packets and Gas," SPIE 2003.

4. Varma, V.K., Tucker, R., Kercel, S., Rose, J., Luo, W., and Zhao, X., "Pipeline Flaw Detection Using Shear EMAT and Wavelet Analysis," GTI's Natural Gas Technologies II, Phoenix, AZ, February 8–11, 2004.
5. Kercel, S.W., Klein, M.B., and Pouet, B., "In-process Detection of Weld Defects Using Laser-based Ultrasonic Lamb Waves," ORNL/TM-2000/346, November 2000.